

Multi-user ISAC through Stacked Intelligent Metasurfaces: New Algorithms and Experiments

Ziqing Wang¹, Hongzheng Liu¹, Jianan Zhang¹, Rujing Xiong¹, Kai Wan¹, Xuewen Qian²,
Marco Di Renzo², Robert Caiming Qiu¹

¹ Huazhong University of Science and Technology, Wuhan, China.

(e-mail: {wangziqing, hongzhengliu, zhangjn, rujing, kai_wan, caiming}@hust.edu.cn).

² Université Paris-Saclay, CNRS, CentraleSupélec, Laboratoire des Signaux et Systèmes, 91192 Gif-sur-Yvette, France
(e-mail: xuewen.qian@centralesupelec.fr, marco.di-renzo@universite-paris-saclay.fr).

Abstract—This paper investigates a Stacked Intelligent Metasurfaces (SIM)-assisted Integrated Sensing and Communications (ISAC) system. An extended target model is considered, where the BS aims to estimate the complete target response matrix relative to the SIM. Under the constraints of minimum Signal-to-Interference-plus-Noise Ratio (SINR) for the communication users (CUs) and maximum transmit power, we jointly optimize the transmit beamforming at the base station (BS) and the end-to-end transmission matrix of the SIM, to minimize the Cramér-Rao Bound (CRB) for target estimation. Effective algorithms such as the alternating optimization (AO) and semidefinite relaxation (SDR) are employed to solve the non-convex SINR-constrained CRB minimization problem. Finally, we design and build an experimental platform for SIM, and evaluate the performance of the proposed algorithms for communication and sensing tasks.

Index Terms—Stacked Intelligent Metasurfaces (SIM), communication, sensing, integrated sensing and communications (ISAC), Cramér-Rao Bound (CRB).

I. INTRODUCTION

Integrated Sensing and Communications (ISAC) has garnered increasing attention recently, driven by the forthcoming deployment of sixth-generation (6G) and subsequent communication systems [1]. With the expansion of frequency bands for 6G networks, ISAC entails the fusion of sensing and communication systems to optimize congested wireless/hardware resources. This integrated approach embraces a symbiotic design paradigm, offering a unified platform for concurrently executing communication and radar sensing functionalities through the transmission of integrated signals [2].

In general, ISAC offers substantial improvements in performance and resource efficiency compared to standalone sensing and communication systems, largely due to the cooperative utilization of wireless resources, radio waveforms, and hardware platforms. However, sensing and communication functions, based on separate information processing principles, lead to various performance tradeoffs between them. These tradeoffs span from information-theoretic limits to physical layer performance considerations, as well as cross-layer design compromises. More precisely, from an information-theoretic viewpoint, the fundamental tradeoff between communication and sensing in ISAC can be mainly classified into two types:

(I) the tradeoff between the subspaces occupied by communication and sensing signals during transmission (ST). The ST tradeoff could be quantified by power allocation approaches across orthogonal or quasi-orthogonal dimensions [3]–[5]. More essentially, the ST tradeoff could also be quantified by assessing the disparity between the span of the “communication subspace” and “sensing subspace” [6], where the eigenspaces of these channels do not align or when the water-filling strategies do not concentrate power on the dominant eigenvectors. (II) The tradeoff between the determinism and randomness of the signals transmitted for communication and sensing (DRT). A larger communication capacity requires more randomness; conversely, higher sensing performance requires less randomness. Therefore, the essence of ISAC lies in the tradeoff between the determinism and randomness of signals [7].

While ISAC effectively mitigates spectrum scarcity, obstacles such as buildings or trees in outdoor settings, as well as furniture or walls in indoor environments, can obstruct signal propagation. Reconfigurable Intelligent Surface (RIS) is regarded as a promising solution for enhancing ISAC systems, because of its unique capability to steer wireless signals to desired destinations without necessitating additional energy or spectrum resources. Different types of RISs have been studied, including reflecting, refracting, and hybrid implementations [8], [9]. A reflective RIS redirects incident signals toward users located on the same side of the base station (BS). In contrast, signals can pass through a refracting (or transmissive) RIS toward users positioned on the opposite side of the BS. As for the hybrid type, the RIS functions dually, facilitating both reflection and refraction functionalities. A hybrid RIS is also referred to as simultaneously reflecting and transmitting reconfigurable intelligent surfaces (STAR-RIS) or intelligent omni-surface (IOS).

As for reflective RIS-assisted ISAC systems, the authors of [10] and [11] jointly optimized the beamforming of both the BS and RIS by using semidefinite relaxation (SDR) and alternating optimization techniques. Since the modeling of a single transmissive RIS and a single reflective RIS is mathematically identical under ideal modeling assumptions, studies on ISAC assisted by a single reflective RIS can be extrapolated to the corresponding transmissive RIS. STAR-

This work was supported by the National Natural Science Foundation of China under Grant 12141107.

RIS-assisted ISAC systems considered in [12] indicated the effectiveness of joint beamforming and the superior gain of STAR-RIS over conventional reflective RIS for ISAC.

Prior studies on RIS-assisted ISAC systems primarily relied on single-layer meta-surface configurations, which resulted in coverage blind spots [13]. A recently proposed technology called stacked intelligent metasurface (SIM), which is comprised of multiple transmissive RIS units arranged in parallel, has been proven to be a potent method for performance improvement at a reduced implementation complexity [14], [15]. Since the multi-layer beamforming in SIM-aided systems enhances the spatial resolution of the primary beam, SIM has been employed to facilitate multi-user communication and Direction of Arrival (DoA) estimation. Nevertheless, there has been no research works exploring SIM-aided ISAC systems and experiments validating the performance of SIM by using hardware platforms.

A. Contributions

The main contributions of this paper are the following:

(1) **Algorithm:** A sub-wavelength SIM model [14] is employed in this paper. Due to the multi-layer structure of the SIM, coupled with the rank-1 constraint for the transmit power for communication and the signal-to-noise ratio constraint for sensing, the optimization problem becomes inherently non-convex. We propose a Multi-Layer Alternating Optimization (MAO) algorithm by using the Singular Value Decomposition (SVD) to relax the optimization problems and develop an efficient solution for them.

(2) **Experiments:** We manufactured three 1-bit transmissive RISs that consist of 16×16 unit cells to construct an SIM, as illustrated in Fig. 4. Also, we conducted experiments in a controlled darkroom environment to validate the performance of the proposed algorithm for SIM-assisted communication-only and sensing-only applications, respectively.

II. SYSTEM MODEL

In this paper, we investigate the SIM-aided ISAC system illustrated in Fig. 1. The formulation of the ISAC system is based on [11], with the main difference that we consider a SIM (i.e., multi-layer transmissive RIS) while [11] considers a single-layer reflective RIS. The ISAC system consists of a BS with $M > 1$ antennas, $K \geq 1$ single-antenna communication users (CUs), and an extended (sensing) target positioned within the Non-Line-of-Sight (NLoS) region of the BS. For the sake of simplicity, we assume that $K \leq M$. The SIM is composed of L metasurface layers, each of which consists of N meta-atoms (unit cells). Let $\mathcal{L} = \{1, \dots, L\}$, $\mathcal{N} = \{1, \dots, N\}$, $\mathcal{K} = \{1, \dots, K\}$ denote the sets of metasurface layers, meta-atoms in each metasurface layer, and the set of users, respectively. According to Rayleigh-Sommerfeld diffraction theory [16], the transmission coefficient from the \tilde{m} -th meta-atom on the $(\ell - 1)$ -th transmissive metasurface

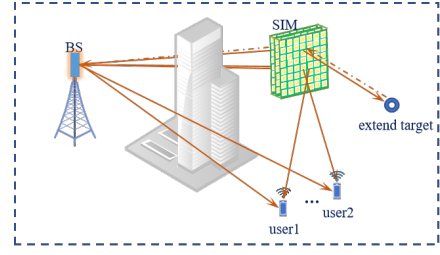


Fig. 1. System model of the considered SIM-aided multi-user ISAC system.

layer to the m -th meta-atom on the ℓ -th transmissive layer is expressed by

$$\omega_{m,\tilde{m}}^\ell = \frac{A_t \cos \chi_{m,\tilde{m}}^\ell}{r_{m,\tilde{m}}^\ell} \left(\frac{1}{2\pi r_{m,\tilde{m}}^\ell} - j \frac{1}{\lambda} \right) e^{j2\pi r_{m,\tilde{m}}^\ell / \lambda}, \quad (1)$$

where $r_{m,\tilde{m}}^\ell$ denotes the transmission distance, A_t denotes the area of the meta-atom, and $\chi_{m,\tilde{m}}^\ell$ represents the angle between the propagation direction and the normal direction of the $(\ell - 1)$ -th transmissive metasurface layer. Let $\Omega_\ell \in \mathbb{C}^{N \times N}$, $\ell \in \mathcal{L}$ denote the diffraction matrix between the ℓ -th transmit metasurface layer and the $(\ell + 1)$ -th transmissive metasurface layer. $\Phi_\ell \in \mathbb{C}^{N \times N}$ denotes the transmission coefficient matrix of the ℓ -th transmissive metasurface layer, where $\Phi_\ell = \text{diag}(\phi_{\ell,1}, \phi_{\ell,2}, \dots, \phi_{\ell,N})$, $\phi_{\ell,n} = e^{j\psi_{\ell,n}}$, with $\psi_{\ell,n} \in [0, 2\pi)$ for each $n \in \mathcal{N}$. Therefore, the end-to-end transmission matrix of the SIM $\mathbf{P} \in \mathbb{C}^{N \times N}$ is expressed as

$$\mathbf{P} = \Phi_L \Omega_{L-1} \Phi_{L-1} \dots \Phi_\ell \Omega_{\ell-1} \dots \Omega_2 \Phi_2 \Omega_1 \Phi_1. \quad (2)$$

We consider a transmission block consisting of T symbols. Let $\mathcal{T} = \{1, \dots, T\}$ denote the set of symbols. Also, let $s_k(t)$ denote the communication signal for CU $k \in \mathcal{K}$ at time instant $t \in \mathcal{T}$ and $\mathbf{w}_k \in \mathbb{C}^{M \times 1}$ denote the transmission beamforming vector. Assume $s_k(t)$ is an independent and identically distributed (i.i.d.) random variable with zero mean and unit variance. The transmitted signal at time instant t is expressed as

$$\mathbf{x}(t) = \sum_{k \in \mathcal{K}} \mathbf{w}_k s_k(t) + \mathbf{x}_0, \quad (3)$$

where $\mathbf{x}_0 \in \mathbb{C}^{M \times 1}$ denotes the signal vector dedicated to sensing at symbol t , generated independently from $s_k(t)$.

Let $\mathbf{h}_{d,k}^H \in \mathbb{C}^{1 \times N}$ denote the channel vector from the BS to CU k for the direct link. Also, let $\mathbf{h}_{r,k}^H \in \mathbb{C}^{1 \times N}$ denote the channel vector from the SIM to CU k and $\mathbf{G} \in \mathbb{C}^{N \times M}$ denote the channel matrix from the BS to the SIM. We assume that the BS has perfect channel state information (CSI) of the link between the BS and the CUs. This can be obtained through well-known channel estimation algorithms. Then the received signal at CU k and the time instant t [17] is

$$\begin{aligned} y_k(t) &= (\mathbf{h}_{d,k}^H + \mathbf{h}_{r,k}^H \mathbf{P} \mathbf{G}) \mathbf{x}(t) + \mathbf{n}_k(t) \\ &= (\mathbf{h}_{d,k}^H + \mathbf{h}_{r,k}^H \mathbf{P} \mathbf{G}) \mathbf{w}_k s_k(t) \\ &\quad + (\mathbf{h}_{d,k}^H + \mathbf{h}_{r,k}^H \mathbf{P} \mathbf{G}) \sum_{i \in \mathcal{K}, i \neq k} \mathbf{w}_i s_i(t) \\ &\quad + (\mathbf{h}_{d,k}^H + \mathbf{h}_{r,k}^H \mathbf{P} \mathbf{G}) \mathbf{x}_0 + \mathbf{n}_k(t), \end{aligned} \quad (4)$$

$$\begin{aligned}
(\text{P1}) : & \min_{\{\mathbf{w}_k\}, \mathbf{R}_0, \mathbf{P}} \text{tr}((\mathbf{PGR}_{ie}\mathbf{G}^H\mathbf{P}^H)^{-1}) \text{tr}((\mathbf{PGG}^H\mathbf{P}^H)^{-1}) \\
\text{s.t.} & \frac{\left| \left(\mathbf{h}_{d,k}^H + \mathbf{h}_{r,k}^H \mathbf{PG} \right) \mathbf{w}_k \right|^2}{\sum_{i \in \mathcal{K}, i \neq k} \left| \left(\mathbf{h}_{d,k}^H + \mathbf{h}_{t,k}^H \mathbf{PG} \right) \mathbf{w}_i \right|^2 + \left(\mathbf{h}_{d,k}^H + \mathbf{h}_{r,k}^H \mathbf{PG} \right) \mathbf{R}_0 \left(\mathbf{h}_{d,k} + \mathbf{G}^H \mathbf{P}^H \mathbf{h}_{r,k} \right) + \sigma_k^2} \geq \Gamma_k, \forall k \in \mathcal{K} \quad (8a) \\
& \sum_{k \in \mathcal{K}} \|\mathbf{w}_k\|^2 + \text{tr}(\mathbf{R}_0) \leq P_0 \quad (8b) \\
& \mathbf{R}_0 \succeq \mathbf{0} \quad (8c) \\
& |\phi_{\ell,n}| = 1, \forall \ell \in \mathcal{L}, \forall n \in \mathcal{N}. \quad (8d)
\end{aligned}$$

where $\mathbf{n}_k(t) \sim \mathcal{CN}(0, \sigma_k^2)$ denotes the additive white Gaussian noise (AWGN) at the CU k .

When transmitting $\mathbf{x}(t)$ for target sensing, the echoed signal matrix at the BS is formulated as

$$\mathbf{y}_s(t) = \mathbf{G}^T \mathbf{P}^T \mathbf{H}_s \mathbf{P} \mathbf{G} \mathbf{x}(t) + \mathbf{n}_R(t), \quad (5)$$

where $\mathbf{H}_s \in \mathbb{C}^{N \times N}$ denotes the target response matrix (i.e., the cascaded channel over the SIM-target-SIM link) and $\mathbf{n}_R(t) \in \mathbb{C}^{M \times 1}$ is the AWGN vector with variance σ_R^2 .

For the extended target, based on [11], the CRB of the estimate of \mathbf{H}_s is

$$\begin{aligned}
\text{CRB}(\mathbf{H}_s) & \\
& = \frac{\sigma_R^2}{T} \text{tr} \left(\left(\mathbf{PGR}_{ie}\mathbf{G}^H\mathbf{P}^H \right)^{-1} \right) \text{tr} \left(\left(\mathbf{PGG}^H\mathbf{P}^H \right)^{-1} \right), \quad (6)
\end{aligned}$$

where $\mathbf{R}_{ie} = \sum_{k \in \mathcal{K}} \mathbf{w}_k \mathbf{w}_k^H + \mathbf{R}_0$ with $\mathbf{R}_0 = \frac{1}{T} \sum_{t \in \mathcal{T}} \mathbf{x}_0 \mathbf{x}_0^H$.

Note that \mathbf{H}_s can be estimated only when $\text{rank}(\mathbf{PG}) = N$ and $\text{rank}(\mathbf{R}_{ie}) \geq N$, otherwise we have $\text{CRB}(\mathbf{H}_s) \rightarrow \infty$. It is apparent that $\text{rank}(\sum_{k \in \mathcal{K}} \mathbf{w}_k \mathbf{w}_k^H) \leq K$, therefore, when $K < N$, we need a dedicated sensing signal vector \mathbf{x}_0 to ensure $\text{rank}(\mathbf{R}_{ie}) \geq N$.

Based on (4), the corresponding SINR of the k -th CU in the extended target case can be formulated as

$$\begin{aligned}
\gamma_k = & \\
& \frac{\left| \mathbf{h}_{d,k}^H + \mathbf{h}_{r,k}^H \mathbf{PG} \mathbf{w}_k \right|^2}{\sum_{i=1, i \neq k}^K \left| \mathbf{h}_{d,k}^H + \mathbf{h}_{r,k}^H \mathbf{PG} \mathbf{w}_i \right|^2 + \left\| \mathbf{h}_{d,k}^H + \mathbf{h}_{r,k}^H \mathbf{PG} \mathbf{x}_0 \right\|^2 + \sigma_k^2}.
\end{aligned}$$

Let P_0 be the maximum transmission power at the BS, the power constraint can be formulated as

$$\mathbb{E}(\|\mathbf{x}(t)\|^2) = \sum_{k \in \mathcal{K}} \|\mathbf{w}_k\|^2 + \text{tr}(\mathbf{R}_0) \leq P_0. \quad (7)$$

Then, we aim to minimize the $\text{CRB}(\mathbf{H}_s)$ for the extended target estimation by jointly optimizing the transmission beamforming matrices $\{\mathbf{w}_k\}$ and \mathbf{R}_0 at the BS, along with the end-to-end transmission matrix \mathbf{P} of the SIM. The optimization problem needs to be solved while satisfying the minimum SINR constraints Γ_k at the CUs and subject to the maximum transmit power constraint at the BS. Consequently, the problem can be formulated as P1. It is worth noting that the SINR constraints in (8a) and the unit-modulus constraints in (8d) render problem P1 non-convex.

III. SIM-AIDED INTEGRATED SENSING AND COMMUNICATIONS

In this section, we aim to solve problem P1. Compared to the joint beamforming for ISAC with a single-layer reflective RIS in [11], the main challenge of the formulated problem resides in the multi-layer structure of the SIM. To address this challenge, we devise an efficient algorithm for problem P1 by employing alternating optimization, to optimize $\{\mathbf{w}_k\}$, \mathbf{R}_0 and the end-to-end transmission matrix \mathbf{P} .

a) *Transmission Beamforming Optimization* $\{\mathbf{w}_k\}$ and \mathbf{R}_0 : First, we optimize $\{\mathbf{w}_k\}$ and \mathbf{R}_0 in P1 assuming that the end-to-end transmission matrix \mathbf{P} of the SIM in (2) is fixed (i.e., assuming that Φ_L, \dots, Φ_1 are fixed). So problem P1 can be transformed as follows:

$$\begin{aligned}
(\text{P1.1}) : & \min_{\{\mathbf{w}_k\}, \mathbf{R}_0} \text{tr}((\mathbf{PGR}_{ie}\mathbf{G}^H\mathbf{P}^H)^{-1}) \text{tr}((\mathbf{PGG}^H\mathbf{P}^H)^{-1}) \\
\text{s.t.} & (8a), (8b), (8c).
\end{aligned}$$

Based on the multi-layer structure of the SIM, we employ a layer-by-layer (i.e., optimizing Φ_L, \dots, Φ_1 alternately) optimization approach for the matrices of transmission coefficient of the layers. The objective function in problem P1.1 can be transformed as

The objective function in problem P1.1 can be transformed as

$$\begin{aligned}
& \text{tr}((\mathbf{PGR}_{ie}\mathbf{G}^H\mathbf{P}^H)^{-1}) \text{tr}((\mathbf{PGG}^H\mathbf{P}^H)^{-1}) \\
& = \text{tr}(\underbrace{(\Phi_L^H \Phi_L)^{-1}}_{\Phi_L \Phi_L^H = \mathbf{I}_N} (\mathbf{A}_L \mathbf{G} \mathbf{R}_{ie} \mathbf{G}^H \mathbf{A}_L^H)^{-1}) \text{tr}((\mathbf{PGG}^H\mathbf{P}^H)^{-1}) \quad (9) \\
& = \text{tr}((\mathbf{A}_L \mathbf{G} \mathbf{R}_{ie} \mathbf{G}^H \mathbf{A}_L^H)^{-1}) \text{tr}((\mathbf{A}_L \mathbf{G} \mathbf{G}^H \mathbf{A}_L^H)^{-1}),
\end{aligned}$$

where $\mathbf{A}_\ell := \Omega_{\ell-1} \Phi_{\ell-1} \dots \Omega_2 \Phi_2 \Omega_1 \Phi_1$, for $\ell \in \{1, 2, \dots, L\}$. Hence, problem P1.1 can be further transformed as follows:

$$\begin{aligned}
(\text{P1.2}) : & \min_{\{\mathbf{w}_k\}, \mathbf{R}_0} \text{tr}((\mathbf{A}_L \mathbf{G} \mathbf{R}_{ie} \mathbf{G}^H \mathbf{A}_L^H)^{-1}) \text{tr}((\mathbf{A}_L \mathbf{G} \mathbf{G}^H \mathbf{A}_L^H)^{-1}) \\
\text{s.t.} & (1 + \frac{1}{\Gamma_k}) \text{tr}(\mathbf{H}_k \tilde{\mathbf{W}}_k) - \text{tr}(\mathbf{H}_k (\sum_{k \in \mathcal{K}} \tilde{\mathbf{W}}_k + \mathbf{R}_0)) \geq \sigma_k^2, \\
& \forall k \in \mathcal{K}, \quad (10a) \\
& \sum_{k \in \mathcal{K}} \text{tr}(\tilde{\mathbf{W}}_k) + \text{tr}(\mathbf{R}_0) \leq P_0, \quad (10b) \\
& \mathbf{R}_0 \succeq \mathbf{0}, \tilde{\mathbf{W}}_k \succeq \mathbf{0}, \forall k \in \mathcal{K}, \quad (10c) \\
& \text{rank}(\tilde{\mathbf{W}}_k) \leq 1, \forall k \in \mathcal{K}, \quad (10d)
\end{aligned}$$

where $\mathbf{h}_k = \mathbf{h}_{d,k} + \mathbf{G}^H \mathbf{A}_L^H \Phi_L^H \mathbf{h}_{r,k}$, $\tilde{\mathbf{W}}_k = \mathbf{w}_k \mathbf{w}_k^H$ and $\mathbf{H}_k = \mathbf{h}_k \mathbf{h}_k^H$. By relaxing the rank-1 constraint in (10d), problem

P1.2 becomes a convex semi-definite program (SDP), which can be solved by convex solvers such as CVX in [18]. The solutions for $\{\tilde{\mathbf{W}}_k^*\}$ and \mathbf{R}_0^* by CVX for problem P1.2 are

$$\mathbf{w}_k^{\text{opt}} = \left(\mathbf{h}_k^H \tilde{\mathbf{W}}_k^* \mathbf{h}_k \right)^{-1/2} \tilde{\mathbf{W}}_k^* \mathbf{h}_k, \forall k \in \mathcal{K}, \quad (11a)$$

$$\mathbf{R}_0^{\text{opt}} = \mathbf{R}_0^* + \sum_{k \in \mathcal{K}} \tilde{\mathbf{W}}_k^* - \sum_{k \in \mathcal{K}} \mathbf{w}_k^{\text{opt}} (\mathbf{w}_k^{\text{opt}})^H. \quad (11b)$$

b) Transmission Coefficient Matrix Φ_L Optimization:

We then optimize the end-to-end transmission matrix \mathbf{P} in problem P1 with fixed $\{\mathbf{w}_k\}$ and \mathbf{R}_0 . The transmission coefficient matrices $\Phi_1, \Phi_2, \dots, \Phi_L$ in \mathbf{P} will be optimized alternately.

Since $\text{CRB}(\mathbf{H}_s)$ in problem P1.2 is independent of the transmission coefficient matrix Φ_L , we find Φ_L with an explicit objective of enhancing the SINR at all CUs [19]. The optimization problem can be formulated as follows:

$$(P1.3) \quad \max_{\Phi_L, \{\varrho_k\}} \quad \sum_{k \in \mathcal{K}} \varrho_k$$

$$\text{s.t.} \quad \left| \left(\mathbf{h}_{d,k}^H + \mathbf{h}_{r,k}^H \mathbf{A}_L \Phi_L \mathbf{G} \right) \mathbf{w}_k \right|^2$$

$$- \Gamma_k \sum_{i \in \mathcal{K}, i \neq k} \left| \left(\mathbf{h}_{d,k}^H + \mathbf{h}_{r,k}^H \mathbf{A}_L \Phi_L \mathbf{G} \right) \mathbf{w}_i \right|^2$$

$$- \Gamma_k \left(\mathbf{h}_{d,k}^H + \mathbf{h}_{r,k}^H \mathbf{A}_L \Phi_L \mathbf{G} \right) \mathbf{R}_0 \left(\mathbf{h}_{d,k}^H + \mathbf{h}_{r,k}^H \mathbf{A}_L \Phi_L \mathbf{G} \right)^H$$

$$+ \mathbf{G}^H \Phi_L^H \mathbf{A}_L^H \mathbf{h}_{r,k} - \Gamma_k \sigma_k^2 \geq \varrho_k, \forall k \in \mathcal{K} \quad (12a)$$

$$\varrho_k \geq 0, \forall k \in \mathcal{K} \quad (12b)$$

$$|\phi_{\ell,n}| = 1, \forall \ell \in \mathcal{L}, \forall n \in \mathcal{N}. \quad (12c)$$

The auxiliary variable ϱ_k represents the difference between the actual SINR of CU k and the threshold Γ_k . Problem P1.3 can be solved by using SDR and Gaussian randomization [19].

c) Transmission Coefficient Matrices $\Phi_{L-1}, \dots, \Phi_1$ Optimization: After updating the transmission coefficient matrix of the L -th layer Φ_L , we optimize the matrix for $(L-1)$ -th layer Φ_{L-1} to the first layer Φ_1 alternately, employing the following procedure. We illustrate how to solve Φ_{L-1} as an example and the remaining transmission coefficient matrices can be solved similarly. Initially, we write the objective function as

$$\text{tr} \left((\mathbf{PGR}_{ie} \mathbf{G}^H \mathbf{P}^H)^{-1} \right) \text{tr} \left((\mathbf{P} \mathbf{G} \mathbf{G}^H \mathbf{P}^H)^{-1} \right)$$

$$= \text{tr} (\Xi_1 \Xi_2) \text{tr} (\Xi_1 \Xi_3), \quad (13)$$

where

$$\Xi_1 = (\Omega_{L-1}^H \Omega_{L-1})^{-1}, \quad (14a)$$

$$\Xi_2 = (\Phi_{L-1} \Omega_{L-2} \dots \Phi_2 \Omega_1 \Phi_1 \mathbf{G} \mathbf{R}_{ie} \mathbf{G}^H (\Phi_{L-1} \Omega_{L-2} \dots \Phi_2 \Omega_1 \Phi_1)^H)^{-1}, \quad (14b)$$

$$\Xi_3 = (\Phi_{L-1} \Omega_{L-2} \dots \Phi_2 \Omega_1 \Phi_1 \mathbf{G} \mathbf{G}^H (\Phi_{L-1} \Omega_{L-2} \dots \Phi_2 \Omega_1 \Phi_1)^H)^{-1}. \quad (14c)$$

Based on the properties of the diffraction matrix Ω_{L-1} , Ξ_1 is a fixed full-rank Hermitian matrix. We denote the singular value decomposition $\Xi_1 = \mathbf{U} \Sigma \mathbf{V}$ with the maximum and minimum singular values denoted by σ_{max} and σ_{min} , respectively, which

are constant. Hence, we have $\sigma_{min} \text{tr}(\Xi_2) \leq \text{tr}(\Xi_1 \Xi_2) = \text{tr}(\Xi_2^{1/2} \Xi_1 \Xi_2^{1/2}) \leq \sigma_{max} \text{tr}(\Xi_2)$. Thus we can take the following relaxation on the objective function in (13)

$$\text{tr}(\Xi_1 \Xi_2) \rightarrow \text{tr}(\Xi_2). \quad (15)$$

Similarly, we can also take the following relaxation on the objective function in (13)

$$\text{tr}(\Xi_1 \Xi_3) \rightarrow \text{tr}(\Xi_3). \quad (16)$$

As a result, the relaxed objective function in (13) becomes $\text{tr}(\Xi_2) \text{tr}(\Xi_3)$, which is independent of Φ_{L-1} . Based on the related objective function:

- we first update $\{\mathbf{w}_k\}$ and \mathbf{R}_0 by problem P1.2, but with the updated objective function $\text{tr}(\Xi_1 \Xi_3) \rightarrow \text{tr}(\Xi_3)$ and with $\mathbf{h}_k = \mathbf{h}_{d,k} + \mathbf{G}^H \mathbf{A}_{L-1}^H \Phi_{L-1}^H \mathbf{h}_{r,k}$, $\tilde{\mathbf{W}}_k = \mathbf{w}_k \mathbf{w}_k^H$ and $\mathbf{H}_k = \mathbf{h}_k \mathbf{h}_k^H$;
- we then obtain Φ_{L-1} by solving P1.3, in which we replace \mathbf{A}_L by \mathbf{A}_{L-1} and Φ_L by Φ_{L-1} .

Similarly, the remaining phase shift matrices $\Phi_{L-2}, \dots, \Phi_1$ are obtained by the same alternating methods. A block diagram of the proposed algorithm is illustrated in Fig. 2.

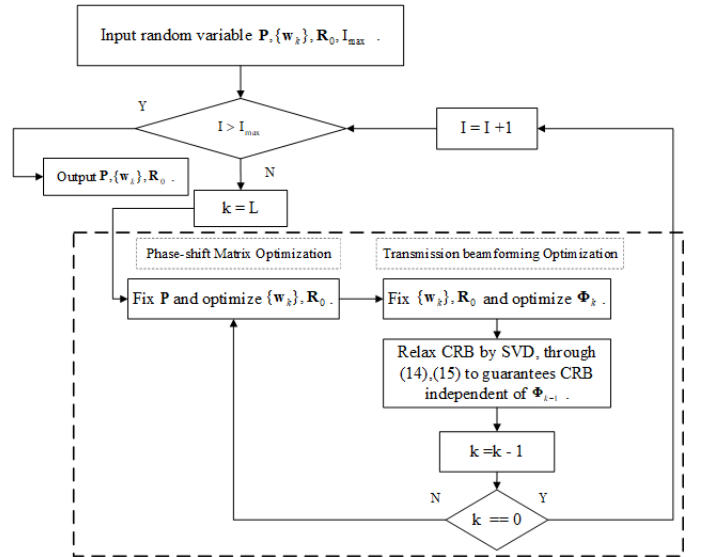


Fig. 2. Multi-layer Alternating Optimization algorithm (MAO). I_{max} represents the maximum number of iterations.

IV. NUMERICAL RESULTS

In this section, numerical results are introduced to evaluate the performance of our proposed algorithm. The distance-dependent path loss is set to $L(d) = L_0 (\frac{d}{d_0})^{-\alpha_0}$, where $L_0 = -30\text{dB}$ denotes the loss at the reference $d_0 = 1\text{m}$ and α_0 denotes the loss exponent. We adopt the Rician fading model for the BS-SIM and SIM-CUs links with the Rician factor equal to 0.5. The coordinates of the BS and the SIM are $(0\text{m}, 0\text{m}, 11\text{m})$ and $(0\text{m}, 0\text{m}, 10\text{m})$, respectively, and two CUs are located at $(0\text{m}, 10\text{m}, 0\text{m})$, $(0\text{m}, 20\text{m}, 0\text{m})$, respectively. The SINR constraint for both CUs is set to $\Gamma \in [0\text{dB}, 30\text{dB}]$. The extended (sensing) target is positioned within the NLoS region of the BS. Other simulation parameters are defined as

follows: $M = N = 4$, $P_0 = 120$ dBm, and $\sigma_R^2 = -120$ dBm noise power. In addition, the thickness of the SIM is set to $T_{\text{SIM}} = 3\lambda$ and the spacing between adjacent transmissive layers of the SIM with L layers is $d_{\text{SIM}} = T_{\text{SIM}}/(L - 1)$.

It can be observed in Fig. 3 that by increasing the number of layers in the SIM leads to an enhanced performance for ISAC. In the figure, specifically, we show the CRB for estimating \mathbf{H}_s with the bias layer via dielectric substrate 3 ($H_3 = 0.2\text{mm}$) through via-holes. The substrate 1 and the substrate 2 layers are designed using F4B materials ($H_1 = H_2 = 2\text{mm}$).

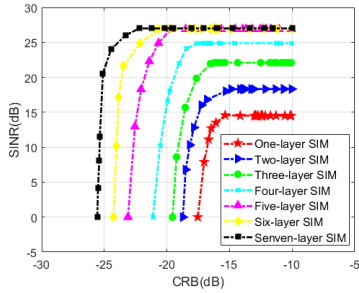


Fig. 3. The CRB for \mathbf{H}_s estimation versus the SINR threshold.

V. EXPERIMENTAL RESULTS

A. The Experimental Platform

In this section, we analyze the performance of SIM by utilizing a new hardware platform. The SIM comprised of multiple transmissive metasurface layers and is shown in Fig. 4a. Each meta-atom of the SIM can apply two phase shifts (1-bit or binary unit cell).

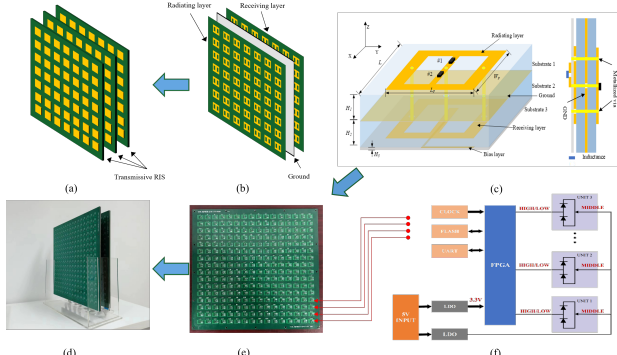


Fig. 4. Stacked Intelligent Metasurface (SIM). (a) The structure of SIM. (b) The structure of a transmissive layer. (c) The structure of a unit cell. (d) 1-bit SIM. (e) 1-bit transmissive layer. (f) Schematic diagram of the logic circuit board.

Each metasurface layer comprises three layers: the radiating layer, the receiving layer, and the ground plane, as depicted in Fig. 4b. Additionally, since the influence of the transmissive plate on signals incident from both sides remains consistent, the structure of the radiating layer and the receiving layer is generally identical. We leverage printed circuit board (PCB) technology to simplify the fabrication process. It embraces the layout of a uniform planar array, comprising 16×16 unit cells, with total size $31 \times 31\text{cm}^2$.

The geometry of each unit cell is illustrated in Fig. 4c, consisting of four copper layers upheld by three substrate layers. The copper layers, arranged from top to bottom, comprise the radiating layer, the ground plane, the receiving layer, and the

bias layer [20]. The radiating layer comprises a rectangular annular patch connected to a rectangular patch, integrated with two PIN diodes (#1 and #2). The outer rectangular annular patch is linked to the ground plane, whereas the rectangular inner patch is connected to the receiving layer via a metalized via-hole. Additionally, the receiving layer is interconnected with the bias layer via dielectric substrate 3 ($H_3 = 0.2\text{mm}$) through via-holes. The substrate 1 and the substrate 2 layers are designed using F4B materials ($H_1 = H_2 = 2\text{mm}$).

The steering-logic board is designed and fabricated as in Fig. 4f. It is powered by a voltage input supply (5V), and an extra low dropout regulator (LDO) provides an external reference voltage for the ground plane (marked as MIDDLE).

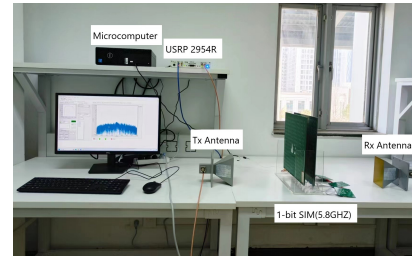


Fig. 5. The SIM-aided communication and sensing prototype system. (The RX serves as the object of sensing or the receiver for communication.)

The experiment system in Fig. 5 uses a Universal Software Radio Peripheral (USRP) as the signal source, transmitting a signal at a frequency of 5.8 GHz with a power of 10 dBm. Each transmission coefficient matrix is derived through an exhaustive search in either communication or sensing experiments. Given the single-antenna system configuration, there is no beamforming scheme employed at the transmitter.

B. Communication Experiment

The transmitted signal passes through a directional transmitter (TX) with an incident angle (relative to the normal) of 15° onto a SIM board located at a distance of 1.75m. From the last transmissive layer of the SIM, the signal exits at a 45° angle (relative to the normal) and travels to the receiver (RX) located at a distance of 7.2m. The USRP was used to process and analyze the received signal. The results are shown in Table I based on the experiment in Fig. 6a.

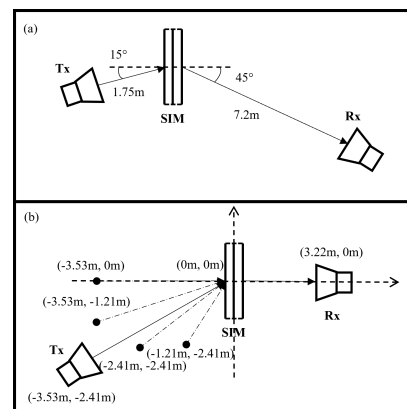


Fig. 6. Scenarios (a) Communication. (b) Sensing.

TABLE I
THE PERFORMANCE OF THE SIM VERSUS THE NUMBER OF LAYERS AND INTER-LAYER SPACING.

Num of layers	$\lambda/4$	$\lambda/2$	λ	$3\lambda/2$	2λ
1-layer	-53dBm	-53dBm	-53dBm	-53dBm	-53dBm
2-layer	-49dBm	-50dBm	-56.5dBm	-55dBm	-55dBm
3-layer	-46dBm	-49dBm	-59dBm	-58dBm	-57dBm

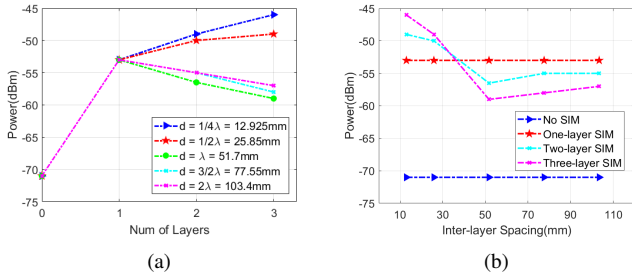


Fig. 7. (a) Impact of the number of layers of the SIM on the communication signal. (b) Impact of the interlayer spacing of the SIM on the communication signal.

It is worth noting that the gain depends on the inter-spacing between adjacent layers, as illustrated in Fig. 7. If the inter-spacing remains equal to or less than half the wavelength, the power at the RX increases with the number of layers. When the inter-spacing exceeds half of the wavelength, the trend of the curve is reversed. The rationale behind this trend is that the longer the inter-distance between the layers the higher the propagation losses between the layers, and the size of each layer of the SIM cannot compensate for the inter-layer attenuation in the considered experiments.

C. Sensing Experiment

TABLE II
DOA ESTIMATION ERROR FOR A DIFFERENT NUMBER OF LAYERS OF THE SIM.

Coordinates of TX	1-layer	2-layer	3-layer
(-3.53m, 0.00m)	4.00°	3.00°	2.50°
(-3.53m, -1.21m)	5.72°	0.22°	1.22°
(-3.53m, -2.41m)	2.71°	1.79°	1.29°
(-2.41m, -2.41m)	3.50°	1.50°	1.50°
(-1.22m, -2.41m)	1.93°	0.93°	0.43°
Average error	3.572°	1.488°	1.388°

The system in Fig. 5 is still utilized for the sensing experiment in Fig. 6b. The experiment assumes fixed positions for both the SIM (0m, 0m) and the RX (3.22m, 0m). The inter-layer distance of the SIM is set to half a wavelength. Five groups of experimental data are collected by changing the position of the TX and the configuration of the SIM. The TX is regarded as a point target, which can be viewed as a special instance of an extended target. The estimated DoA is then derived using the least squares estimator. The positions of the TX and the corresponding estimation errors are presented in Tab. II. We observe that error for DoA estimation decreases with the number of transmissive layers of the SIM.

VI. CONCLUSION

This paper investigated an ISAC scenario with multiple communication users and an extended target. We proposed an

optimization algorithm to jointly optimize the beamforming at the BS and the end-to-end transmission matrix of the SIM. Also, we have built a hardware platform for SIM and evaluated its performance through experiments. Numerical and experimental results demonstrated that the increasing number of layers in the SIM can improve the ISAC performance.

REFERENCES

- [1] A. Liu, Z. Huang *et al.*, "A survey on fundamental limits of integrated sensing and communication," *IEEE Communications Surveys & Tutorials*, vol. 24, no. 2, pp. 994–1034, 2022.
- [2] F. Liu, Y. Cui *et al.*, "Integrated sensing and communications: Toward dual-functional wireless networks for 6G and beyond," *IEEE Journal on Selected Areas in Communications*, vol. 40, no. 6, pp. 1728–1767, 2022.
- [3] H. Hua, T. X. Han *et al.*, "MIMO integrated sensing and communication: CRB-rate tradeoff," *IEEE Transactions on Wireless Communications*, 2023.
- [4] F. Liu, Y.-F. Liu *et al.*, "Cramér-Rao bound optimization for joint radar-communication beamforming," *IEEE Transactions on Signal Processing*, vol. 70, pp. 240–253, 2021.
- [5] F. Liu, C. Masouros *et al.*, "MU-MIMO Communications with MIMO Radar: From Co-existence to Joint Transmission," *IEEE Transactions on Wireless Communications*, vol. 17, no. 4, pp. 2755–2770, 2019.
- [6] M. Ahmadipour, M. Kobayashi *et al.*, "An information-theoretic approach to joint sensing and communication," *IEEE Transactions on Information Theory*, 2022.
- [7] S. Lu, F. Liu *et al.*, "Random ISAC signals deserve dedicated precoding," *arXiv preprint arXiv:2311.01822*, 2023.
- [8] Y. B. Li, L. L. Li *et al.*, "Transmission-type 2-bit programmable metasurface for single-sensor and single-frequency microwave imaging," *Scientific reports*, vol. 6, no. 1, p. 23731, 2016.
- [9] S. Zhang, H. Zhang *et al.*, "Beyond intelligent reflecting surfaces: Reflective-transmissive metasurface aided communications for full-dimensional coverage extension," *IEEE Transactions on Vehicular Technology*, vol. 69, no. 11, pp. 13 905–13 909, 2020.
- [10] X. Song, D. Zhao *et al.*, "Joint transmit and reflective beamforming for IRS-assisted integrated sensing and communication," in *2022 IEEE Wireless Communications and Networking Conference (WCNC)*. IEEE, 2022, pp. 189–194.
- [11] X. Song, X. Qin *et al.*, "Cramér-Rao Bound Minimization for IRS-Enabled Multiuser Integrated Sensing and Communications," *arXiv preprint arXiv:2306.17493*, 2023.
- [12] Z. Liu, X. Li *et al.*, "Toward STAR-RIS-Empowered Integrated Sensing and Communications: Joint Active and Passive Beamforming Design," *IEEE Transactions on Vehicular Technology*, 2023.
- [13] Q. Wu and R. Zhang, "Beamforming optimization for wireless network aided by intelligent reflecting surface with discrete phase shifts," *IEEE Transactions on Communications*, vol. 68, no. 3, pp. 1838–1851, 2019.
- [14] J. An, C. Xu *et al.*, "Stacked intelligent metasurfaces for efficient holographic MIMO communications in 6G," *IEEE Journal on Selected Areas in Communications*, 2023.
- [15] J. An, M. Di Renzo, M. Debbah, and C. Yuen, "Stacked intelligent metasurfaces for multiuser beamforming in the wave domain," in *ICC 2023-IEEE International Conference on Communications*. IEEE, 2023, pp. 2834–2839.
- [16] X. Lin, Y. Rivenson *et al.*, "All-optical machine learning using diffractive deep neural networks," *Science*, vol. 361, no. 6406, pp. 1004–1008, 2018.
- [17] C. Pan, G. Zhou, K. Zhi, S. Hong, T. Wu, Y. Pan, H. Ren, M. Di Renzo, A. L. Swindlehurst, R. Zhang *et al.*, "An overview of signal processing techniques for ris/irs-aided wireless systems," *IEEE Journal of Selected Topics in Signal Processing*, vol. 16, no. 5, pp. 883–917, 2022.
- [18] M. Grant, "CVX: MATLAB software for disciplined convex programming," <http://cvxr.com/cvx>, 2008.
- [19] Q. Wu and R. Zhang, "Intelligent reflecting surface enhanced wireless network via joint active and passive beamforming," *IEEE transactions on wireless communications*, vol. 18, no. 11, pp. 5394–5409, 2019.
- [20] J. Zhang, R. Xiong *et al.*, "Design and Prototyping of Transmissive RIS-Aided Wireless Communication," *arXiv preprint arXiv:2402.05570*, 2024.